The Atomistic Structures of $MgO/SrTiO_3(001)$ and $BaO/SrTiO_3(001)$ Using Simulated Amorphization and Recrystallization

Dean C. Sayle*

Department of Environmental and Ordnance Systems, Cranfield University, Royal Military College of Science, Shrivenham, Swindon UK, SN6 8LA

Graeme W. Watson

Department of Chemistry, Trinity College, Dublin 2, Ireland

Received: September 22, 2000; In Final Form: February 1, 2001

Large-scale atomistic simulations of oxide interfaces have been performed where the thin film is forced to undergo a controlled amorphous transition prior to recrystallizing. The $MO/SrTiO_3(001)$ (M = Ba or Mg) systems explored using this simulation technique demonstrate markedly different structural characteristics owing to the difference in lattice parameter associated with each system. In particular regions of $SrTiO_3(001)$ (TiO_2 terminated) supported MgO undergo a transformation into a pseudohexagonal type structure, reducing the lattice misfit from +7.4% to ca. −0.5 to −4%, whereas the +34% lattice misfit associated with the $BaO/SrTiO_3$ system is reduced to −0.3% via a 45° rotation of the BaO with respect to the underlying $SrTiO_3$. Moreover, the plane exposed by the $SrTiO_3(001)$ support (either SrO or TiO_2) exacts a critical influence on the structure of the thin film. In particular, BaO, when supported on a TiO_2 terminated $SrTiO_3$, comprises a high concentration of dislocations. Conversely, for the analogous SrO terminated system no dislocations are present within the thin film.

Introduction

The chemical, physical and mechanical properties of a material can change tremendously when supported on a substrate material. Indeed, the exploitation of such a phenomenon remains central to applications spanning, catalysis, sensors, electronics, optics and even engineering systems. Clearly, it is desirable to optimize the material properties and to help achieve this goal one must first understand the mechanisms that operate when a material is supported.[1,2]

In previous studies, we explored, using atomistic simulation, the structure of ultrathin incommensurate heteroepitaxial systems,[3] specifically MO/M′O(001), (M,M′=Mg, Ca, Sr, Ba). Here we extend this work by modeling ultrathin metal oxides supported on a perovskite-structured substrate. In particular, we consider the $MgO/SrTiO_3(001)$ and $BaO/SrTiO_3(001)$ systems; $SrTiO_3(001)$ has been widely employed as a substrate suitable for the epitaxial growth of high T_c superconducting films.[1]

In contrast to our previous work, the perovskite (001), employed as a substrate, has the added complexity of offering two surfaces on which to support the thin film. These include the SrO or TiO_2 terminated surfaces. Experimentally, Kawasaki and co-workers fabricated an atomically flat $SrTiO_3(001)$ surface terminated solely by TiO_2.[4] Accordingly, since either surface can be selectively constructed, it is pertinent to ask which surface delivers the better or more appropriate thin film for the particular application. To this end, we focus on the structural characteristics associated with supporting a metal oxide (BaO or MgO) on either a TiO_2 or an SrO terminated $SrTiO_3(001)$ substrate.

To generate realistic models of supported oxide thin films one must consider various factors including the epitaxial relationships, defects and reduced interfacial ion densities. The defects, which evolve in response to misfit accommodation, may include dislocation arrays, vacancies, substitutions, and interstitials including clustering of such defects. Inclusion of some or all of these structural features is clearly a challenging undertaking, but nevertheless must be achieved if one is to generate a realistic model. Many simulations are based upon constructing a trial system, which is then simulated using static or dynamical methods. However, such an approach is not appropriate here since, for example, the nature, location and indeed concentration of the dislocations arrays and associated defects presents a prohibitively high number of permutations to consider. In addition, the inclusion of a dislocation will influence the structure of neighboring dislocations. Essentially, the synergy of interaction of each of the component structural features must also be included within the model. Accordingly, a simulation methodology: "simulated amorphization and recrystallization" has been developed[5] in which all the structural features that would be present within the "real" system are allowed to evolve within the simulation model including the epitaxial relationships and reduced interfacial ion densities. In particular, the overlayer is forced initially to undergo an amorphous transition, which then recrystallizes facilitating the evolution of the structural features including their synergistic interactions.

The amorphization is induced by straining the supported thin film under high compression. The application of high-temperature dynamical simulation to this strained system results in the amorphization of the thin film overlayer (typically within a picosecond of time). Prolonged dynamical simulation is required to allow the system to recrystallize under the influence of the support. We emphasize that this methodology does not parallel

* Corresponding author. E-mail: sayle@rmcs.cranfield.ac.uk.

10.1021/jp0034325 CCC: $20.00
Published on Web 05/12/2001

TABLE 1: Duration of the Dynamical Simulation, Thin Film (TF) Interface Energies, "Bulk" Misfit (based upon the natural lattice parameter of the supported material), Structural Features Observed within the Supported Thin Film and Corresponding "Local" Misfit, and Graphic Illustrating the Structural Modification and Average nearest Neighbor (NN) Metal Oxide Distances within the Supported Thin Film for $MO/SrTiO_3(001)$ (M = Mg, Ba) Systems with the $SrTiO_3(001)$ Support Terminated Either by SrO or TiO_2 Planes

system	$SrTiO_3$ termination	dyanamical simulation	TF energy(Jm^{-2})	"bulk"misfit	features and "local" lattice misfit	graphic	NN M−O distances (Å)
$MgO/SrTiO_3$	SrO	265 ps, 2200 K	4.6	+7%	dislocations	Figures 2, 3	2.05
					coherent regions (< +7%)	Figure 4a	(1.95−2.2)
					incoherent regions (−5%)		
	TiO_2	310 ps, 2200 K	3.1	+7%	coherent (< +7%)		2.01
					pseudohexagonal	Figures 5, 9	(1.95−2.1)
					MgO (−0.5 to −4%)		
					cubic MgO		
$BaO/SrTiO_3$	SrO	145 ps, 600 K	1.9	+34%	45° rotation of	Figures 6, 11	2.75
					BaO (−0.3% misfit)		
					fully coherent		(2.65−2.85)
					many defects (vacancies and interstitials) and defect clusters	Figures 11, 12	
					no dislocations		
	TiO_2	210 ps, 600 K	1.5	+34%	45° rotation of	Figure 13c	2.74
					BaO (−0.3% misfit)		
					fully coherent		(2.55−2.95)
					dislocations	Figure 15	

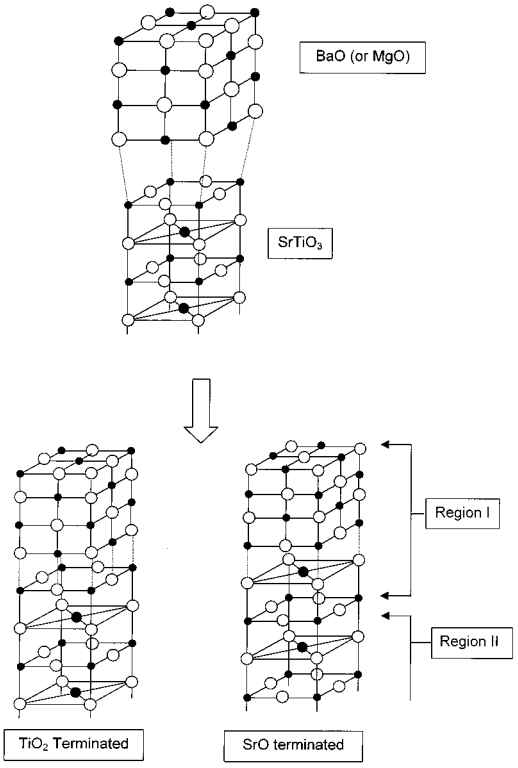

Figure 1. Diagrammatic representations of the initial (before amorphization) interfacial configurations for $MO/SrTiO_3(001)$ (M = Ba, Mg) depicting either the SrO or TiO_2 surface terminations for the $SrTiO_3$ substrate. Barium, magnesium and titanium are represented by the smaller filled spheres, oxygen, the hollow spheres and strontium the larger filled spheres.

recrystallization within "real" systems; rather, it is purely a simulation technique to derive low energy structures and the structural evolution of the system bears no physical significance. The main driving force to the amorphization is the strain under which the thin film is constrained, while the temperature at which the dynamical simulation is run is secondary to inducing amorphization. For example, the procedure can be performed equally as well at 20 K as at 2000 K. However, the recrystallization process at 20 K is much slower. In essence, the optimum temperature is one that allows the structure to evolve but that

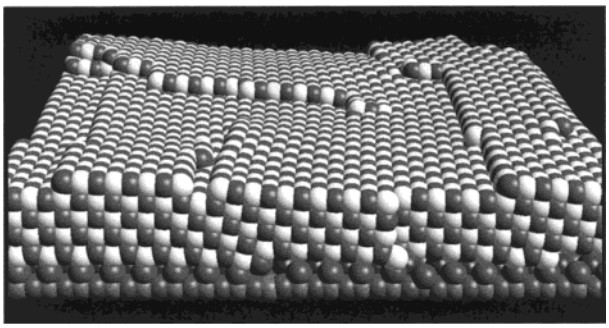

Figure 2. Final interfacial configuration for the $MgO/SrTiO_3(001)$ (SrO terminated) system. Slightly less than 25% of the simulation cell is depicted to maintain clarity of the figure. Magnesium species are represented by the white spheres, oxygen the darker spheres. Only one repeat unit of the underlying $SrTiO_3(001)$ is shown for reasons of clarity.

falls short of melting the thin film. This would be detrimental as it would prevent recrystallization and require an additional quenching step.[5] An important feature of the methodology is that the amorphous transition enables all memory of the preparatory configuration to be lost (radial distribution functions for the amorphous thin film are broad[5] indicating no long range ordering) and therefore the final structures cannot reflect artificially the starting structure. The recrystallization is deemed complete when the system is no longer evolving structurally or energetically, the duration of which is system dependent. In addition, dynamical simulation, as applied to an amorphous structure, allows a more comprehensive exploration of the configurational space, which is likely to result in an energetically more favorable, and hence more realistic, final interface structure.

Methodology

The reliability of any simulation rests ultimately with the potential parameters.[6] Our calculations are based on the Born model of the ionic solid in which the ions interact via long-range Coulombic interactions and short-range parameterized interactions. To calculate the Coulombic interactions, we employ the method of Ewald,[7] which transforms the slowly convergent Coulomb sum in real space into two rapidly convergent sums in real and reciprocal space. In this study we have employed

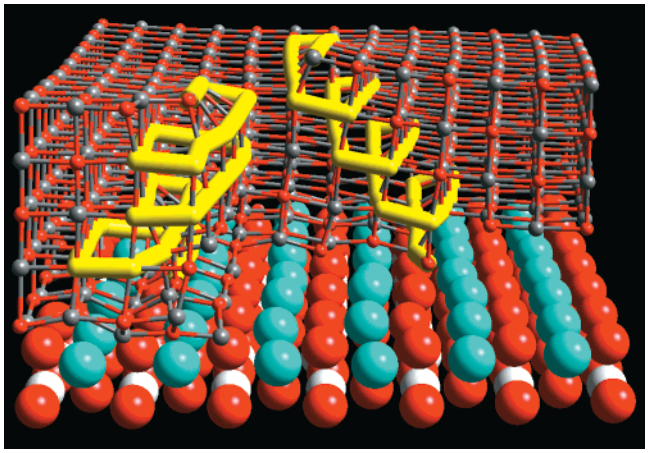

Figure 3. Structural representation of two screw-edge dislocations within the $MgO/SrTiO_3(001)$ (SrO terminated) system. The MgO thin film is represented as a ball-and-stick model with the core structure of the dislocations (stick model) colored yellow. Much of the MgO has been "cut away" to ensure clarity of the relative positions of the dislocation cores within the MgO lattice. The underlying $SrTiO_3$ is depicted using a sphere model representation. Oxygen is colored red, magnesium is gray, strontium is blue, and titanium is white.

the potential parameters of Lewis and Catlow[8] with the additional approximation of the rigid ion model, imposed to reduce the computational expense. The potential parameters have been extensively employed previously to model structures, which have nonoptimal geometries, with good correlation to experiment.[1] These include, for static simulations, interfacial defects,[9] dislocations[10] and grain-boundaries[1,11] and for dynamical simulations, interfacial structures,[12] and surface defects.[13] We suggest therefore that the potential parameters are well suited to explore supported metal-oxide thin films, which may include many structural defects.

In this study, we employ the DL_POLY code,[14] which performs simulations periodic in three dimensions and so we include a void to represent the vacuum above the free surface. The size of the void for the $MgO/SrTiO_3$ system was ca. 80 Å, whereas for the $BaO/SrTiO_3$ the void was ca. 65 Å. Our simulations are facilitated by dividing the calculation into two regions. Region I contains the thin film and the first few layers of the support and is allowed to move during the dynamical simulation. Region II contains a fixed region of the support, which provides the correct crystalline environment. The reason for using the DL_POLY code is that it offers a considerable speed advantage for our particular simulations: The extra computation, due to the inclusion of the void, is less severe since we consider simulation cells with very large surface areas. Consequently, the void direction is our smallest vector and so the computational cost of including a void direction is more than offset by the computational efficiency of a 3-D compared with a 2-D Ewald summation of the Coulombic interactions.[15]

Thin Film Construction. There exists two major difficulties with simulating interfaces at the atomistic level. First, the simulation cell must be sufficiently large to accommodate the incommensurate nature of the system,[16,17] and include misfit induced structural modifications such as dislocations.[18,19] Second, the final structure must not be influenced artificially by the starting structure.[12] To address both concerns we have performed large-scale atomistic simulations, which approach the mesoscale and, in addition, force the supported thin film to undergo an amorphous transition prior to recrystalizing.

Various mechanisms for the amorphization have been explored. These include performing dynamical simulation at very high temperatures to effectively melt the thin film, and constraining the thin film under conditions of compression or tension; under dynamical simulation, the considerable strain within the thin film results in an amorphous structure. Once an

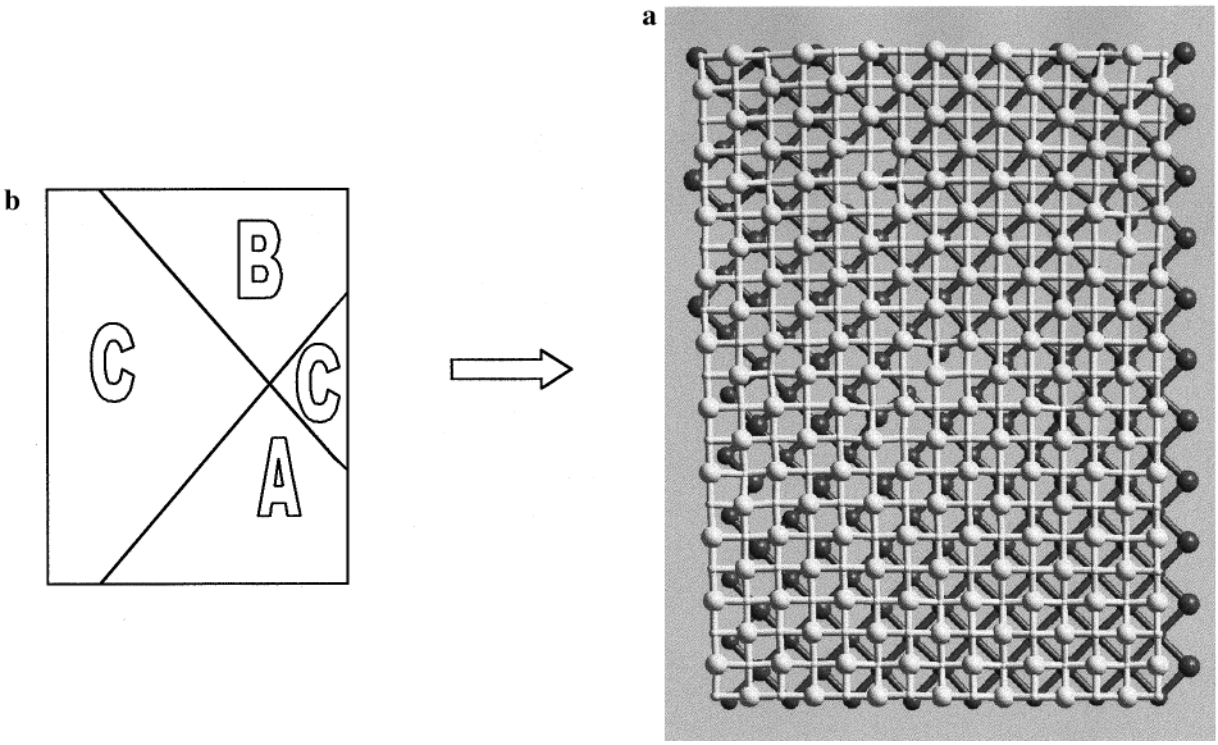

Figure 4. (a) Ball and stick representations of the interfacial MgO and SrO planes at the $MgO/SrTiO_3(001)$ (SrO terminated) interface. Only ca. 5% of the total simulation cell is depicted. Oxygen (MgO) is represented by the larger white sphere, magnesium the smaller white sphere, oxygen ($SrTiO_3$) the larger dark sphere and strontium, the smaller dark sphere. To aid structural interpretation of the figure, (b) depicts a graphic identifying three distinct areas showing the two coherent regions ("A" and "B") separated by a commensurate region ("C").

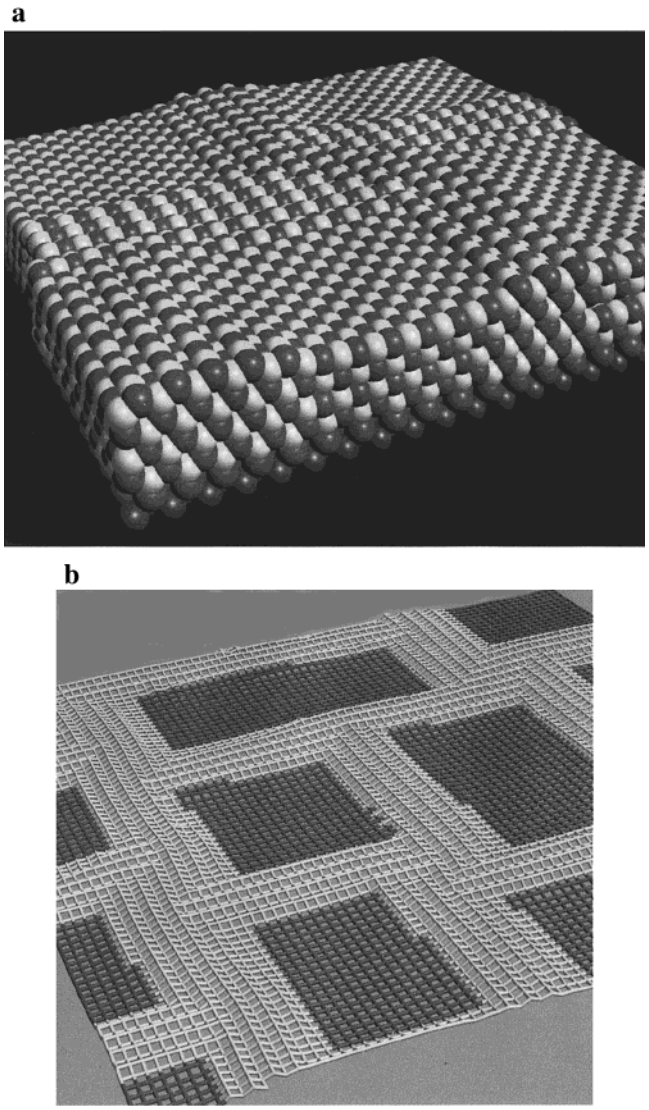

Figure 5. Final interfacial configuration for the $MgO/SrTiO_3(001)$ (TiO_2) terminated system; (a) sphere representation of just under 25% of the full simulation cell. Magnesium species are represented by the white spheres, oxygen the darker spheres. Only one repeat unit of the underlying $SrTiO_3(001)$ is shown for reasons of clarity; (b) stick model of the surface MgO layer (full simulation cell depicted) showing regions of MgO which accommodate the cubic rocksalt type structure (dark region) and regions where the MgO conforms to some kind of "pseudohexagonal" type configuration (light regions).

amorphous structure has been generated, long-duration dynamical simulation facilitates recrystallization of the thin film enabling various structural modifications such as dislocations to evolve. In this present study, we induce amorphicity by constraining the thin film to accommodate the lattice parameter of the substrate. Accordingly, both the MgO and BaO thin films are initially under compression.

The $MO/SrTiO_3$ systems were constructed (M = Mg, Ba) by placing the thin film on top ("cube-on-cube") of a 40×40 $SrTiO_3$ support, which corresponds to 40 $SrTiO_3$ repeat units for each side of the simulation cell giving a surface area of ca. 24400 $Å^2$. For each system, four layers of the MO were placed on the support, in which the metal and oxygen ions were constrained to occupy positions directly above their respective counterions of the underlying $SrTiO_3$. Since the metal oxide is coherent (initially) with respect to the support, it accommodates the full lattice misfit ($MgO/SrTiO_3(001) = +7.4\%$; $BaO/SrTiO_3(001) = +34\%$ misfit), while the $SrTiO_3$ support is maintained

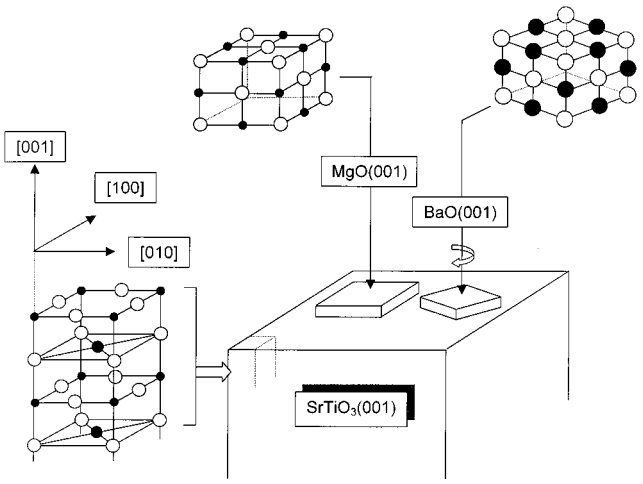

Figure 6. Graphical representations depicting the relative final orientations of the MgO and BaO with respect to the underlying $SrTiO_3(001)$ support.

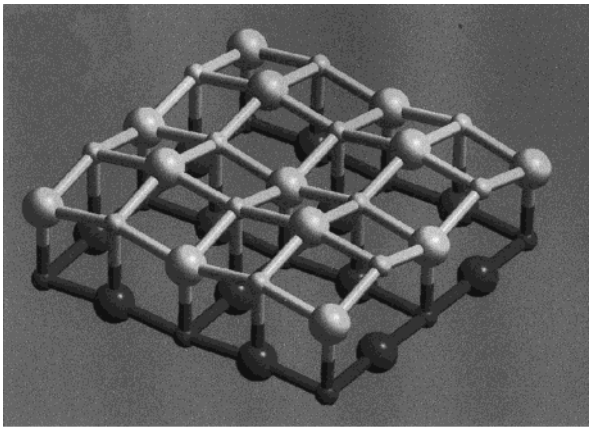

Figure 7. Ball and stick representation of a small region within the $MgO/SrTiO_3(001)$ (TiO_2) terminated system depicting the interfacial MgO and TiO_2 planes. In this particular region, the MgO ions demonstrate a *rumpled* configuration. Oxygen (MgO) is represented by the large white spheres, magnesium the smaller white spheres, oxygen ($SrTiO_3$) the larger dark spheres and titanium the smaller dark spheres.

at its natural lattice parameter. Figure 1 shows graphically the initial configuration of the four systems. We note that since the thin film undergoes an amorphous transition, no significance should be attributed to the initial configurations, since the systems loose all memory of their preparatory configurations. Rather, they are constructed in this way to facilitate the amorphous transition.

Region I, in which all the ions are allowed to move, comprised the thin film and two $SrTiO_3(002)$ layers (one repeat unit) of the support, while region II (ions held fixed) comprised four $SrTiO_3(002)$ layers (two repeat units). Upon dynamical simulation the considerable compressive strain within the supported thin film results in its amorphization, which, upon prolonged dynamical simulation recrystallizes.

Dynamical simulation, with a time step of 5×10^{-3} ps, was performed on each system, first at high temperature and then at 0K, the latter acts effectively as an energy minimization. The duration of the dynamical simulation (Table 1) was sufficient to ensure the recrystallization process was complete and the structure was no longer evolving (the energy of the system had converged). Velocity scaling, performed at every step, was used throughout to prevent the rapid and large build up of excess kinetic energy as the thin film evolves, via an amorphous

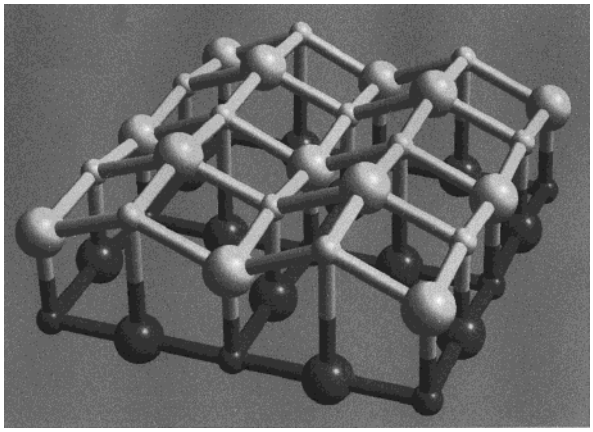

Figure 8. Ball and stick representation of a small region within the $MgO/SrTiO_3(001)$ (TiO_2) terminated system depicting the interfacial MgO and TiO_2 planes. Here, the MgO ions demonstrate a *corrugated* configuration. Oxygen (MgO) is represented by the large white spheres, magnesium the smaller white spheres, oxygen ($SrTiO_3$) the larger dark spheres and titanium the smaller dark spheres.

transition, from the highly strained initial configuration, to a crystalline phase with reduced strain and a range of defects.

For the supported thin film we define a thin film (TF) interface energy following Sayle et al.,[20] which is given by:

$$\gamma_{\text{TF interface}} = (E_{\text{TF interface}} - E_{\text{bulk}}\text{-}n(E_{\text{TF}}))/\text{area},$$

where $E_{\text{TF interface}}$ is the total energy of the interface, E_{bulk}, the bulk energy of the substrate, E_{TF}, the standard three-dimensional periodic bulk energy for the supported thin film material per formulation unit, and n is the number of formula units of the supported thin film.

Results

We first consider the $MgO/SrTiO_3(001)$ system, which is associated with a lattice misfit of +7.4%.

$MgO/SrTiO_3(001)$: SrO Terminated. The interfacial structure for the $MgO/SrTiO_3(001)$ (SrO terminated) is depicted in Figure 2. Only a quarter of the full simulation cell is shown to maintain clarity of the figure. However, the segment presented is of sufficient size to provide adequately a flavor of the full simulation cell. The supported MgO thin film accommodates the rocksalt type structure and exposes the (001) plane at both the interface and the surface of the thin film. The number of layers within the MgO thin film is 4−5 and therefore the surface of the MgO thin film is not atomically flat; rather the surface comprises many steps. The average nearest neighbor Mg−O bond distances within the MgO thin film, derived by calculating the radial distribution function (RDF) for the thin film, is 2.05 Å. This is in accord with an experimental study by Chern and Cheng who found direct evidence to suggest that "the MgO forms with nearly relaxed lattice constant from the first monolayer".[21]

Dislocations. Inspection of the surface of the thin film suggests the presence of dislocations within the supported MgO lattice, which evolve to help accommodate the lattice misfit associated with the system. To aid structural interpretation of the dislocations, the core structure of two neighboring dislocations have been deconvoluted using graphical techniques and are presented in Figure 3. The dislocations have both screw and edge components and are similar to those observed in previous studies.[20]

Defects. The interfacial SrO and underlying TiO_2 planes accommodate many isolated oxygen and strontium vacancies including vacancy association. In addition intermixing of cations across the interface is observed: strontium ions migrate to accommodate magnesium lattice positions within the interfacial MgO plane and the magnesium ions displaced accommodate strontium lattice positions within the interfacial SrO plane.

Epitaxy. Figure 4a depicts a small region, (1235 $Å^2$ in size or ca. 5% of the total simulation cell) showing the MgO and SrO planes either side of the interfacial plane. To aid interpreta-

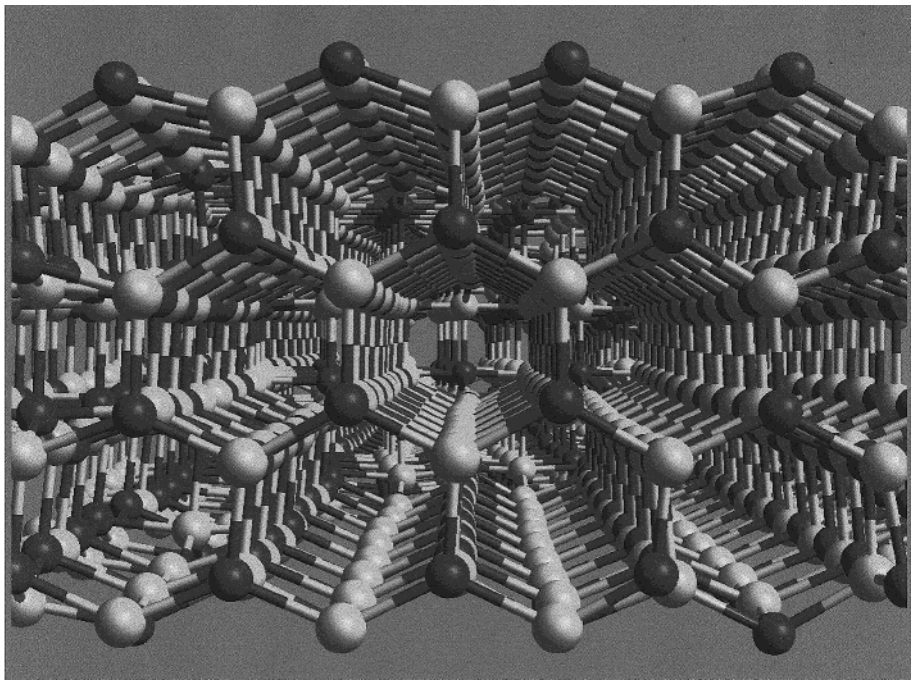

Figure 9. Ball and stick representation (with perspective) of a side view of the $MgO/SrTiO_3(001)$ (TiO_2) terminated system depicting only the MgO thin film illustrating the "pseudohexagonal" type structure adopted by the supported MgO thin film. Part of the interconnecting cubic MgO can also be seen when one views through the central hexagonal pipe.

tion of the structure, a schematic, Figure 4b, identifies three areas labeled "A", "B", and "C".

In region A, the MgO lies coherent with respect to the underlying SrO with the magnesium sublattice lying directly above the Sr and O species of the SrO layer. Interfacial bond distances are calculated to be ca. 2.25 Å for Mg−O and 3.00 Å for Mg−Sr, the magnesium sublattice therefore (on side view) appears corrugated, whereas the Sr and O species in the underlying SrO plane are coplanar.

In region B, the MgO again lies coherent with respect to the underlying SrO although in contrast to region A, the oxygen sublattice of the MgO lies directly above the Sr and O species of the underlying SrO. Interionic distances are calculated to be ca. 3.4 and 3.9 Å for O−Sr and O−O, respectively. Commensurate regions C adjoin the two coherent regions. Within the coherent regions the associated lattice misfit is ca. +7%; whereas the lattice misfit associated locally within the adjoining commensurate regions is ca. −5%. To calculate the latter value, the commensurate relationship between the MgO and underlying $SrTiO_3$ was estimated by inspection of the structure and assigned to a particular near coincidence site lattice.[22]

We now consider MgO supported on the TiO_2 terminated $SrTiO_3(001)$.

$MgO/SrTiO_3(001)$: TiO_2 Terminated. The interfacial structure for the $MgO/SrTiO_3(001)$ (TiO_2 terminated) is depicted in Figure 5a. Again, for reasons of clarity, only a quarter of the full simulation cell is shown. The supported MgO thin film accommodates the rocksalt type structure and exposes the (001) plane at both the interface and the surface of the thin film. The number of layers within the MgO thin film is four; the surface of the thin film is atomically flat (albeit corrugated in certain regions) in contrast to the $MgO/SrTiO_3$(SrO terminated) system. Moreover, the MgO thin film contains no dislocations: We tentatively suggest (surprisingly) that the critical thickness for dislocation evolution for TiO_2 terminated thin films is larger than that SrO terminated systems. In particular, the MgO thin film is able to accommodate the lattice misfit via a remarkable structural transformation.

Close inspection of the MgO thin film structure reveals regions of the MgO, which accommodate a pseudohexagonal type structure. Similar structures have been observed previously.[3] To aid structural interpretation, Figure 5b depicts the surface layer of the MgO thin film. The darker regions represent MgO, which have the normal cubic rocksalt type structure, while for the lighter regions, the MgO accommodates a pseudohexagonal type structure. Close inspection reveals an interconnecting (90 degrees) network of hexagonal pipes. We now look in detail at how such a transformation is able to help accommodate the lattice misfit and begin by considering the epitaxial features associated with the system.

Epitaxy. Inspection of the MgO and TiO_2 interfacial layers reveals the MgO lies coherent with respect to the underlying TiO_2. In particular, the magnesium sublattice of the MgO lies directly above the oxygen sublattice of the TiO_2 plane and 50% of the oxygen sublattice (MgO) lies above the titanium sublattice (Figure 6). In addition, there exists two different interfacial structural configurations. For the first, the MgO exhibits rumpling of the ions within the MgO interfacial plane (Figure 7) and MgO planes directly above these regions accommodate a cubic rocksalt type structure. In contrast, other regions demonstrate a corrugated type structure (Figure 8). Here, the overlying MgO is pseudohexagonal (Figure 9).

Corrugated Regions. For the MgO thin film to maintain a coherent structure with respect to the underlying $SrTiO_3(001)$ necessitates a 7.4% reduction in the MgO lattice parameter, based upon MgO and Ti−O bond distances of 2.1 and 1.95A, respectively. Clearly, the strain within the MgO thin film associated with such a configuration is considerable. Accordingly, to reduce the strain, the MgO subtends an angle, Θ, which ranges from ca. 126 to 138°, about the O−Mg−O (Figures 8 and 10) in the [010] direction and ca. 160−170° along the [100]. This gives rise to the 'corrugated' interfacial MgO and the pseudohexagonal MgO thin film structure. The associated lattice misfit is calculated, based upon the corrugated structure, to range from ca. −0.5 to −4% along the [010]. We suggest the MgO exhibits a 'concertina' effect in certain regions, thereby accommodating the lattice misfit.

Rumpled Regions. Regions of MgO, which retain the cubic structure, must accommodate fully the +7.4 lattice misfit to

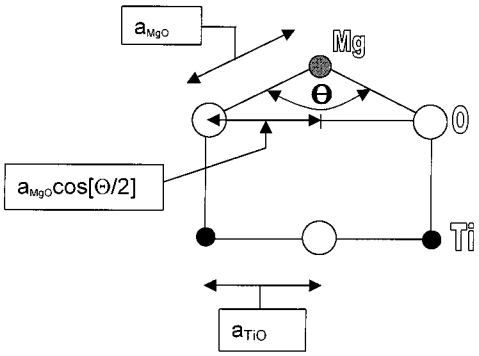

Figure 10. Representation illustrating how the angle, (Θ), subtended about the O−Mg−O bond ([010] direction) leads to a reduction in the local lattice misfit. The misfit is calculated as

$$\text{misfit} = \frac{2|a_{MgO}\cos\left(\frac{\Theta}{2}\right) - a_{TiO}|}{a_{MgO}\cos\left(\frac{\Theta}{2}\right) + a_{TiO}}$$

where a_{MgO} and a_{TiO} are the natural Mg−O and Ti−O bond distances, respectively.

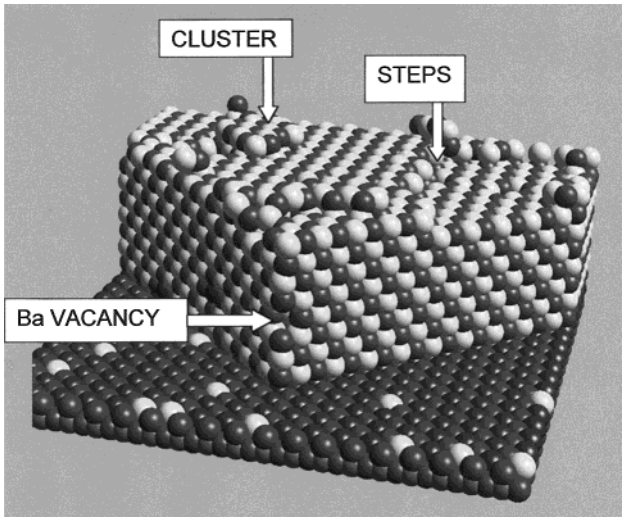

Figure 11. Sphere representation of the $BaO/SrTiO_3(001)$ (SrO terminated) system. Only a small part of the full simulation cell is depicted for reasons of clarity. In addition, part of the overlying BaO thin film has been cut away to demonstrate more clearly, the 45° rotation of the BaO lattice with respect to the underlying $SrTiO_3$. The figure also indicates the presence of BaO clusters and steps on the surface of the thin film and the location of a vacancy within the BaO lattice. Notice also the barium ions accommodating strontium positions within the interfacial SrO layer of the $SrTiO_3$ support. Barium is represented by the white spheres, oxygen the dark spheres.

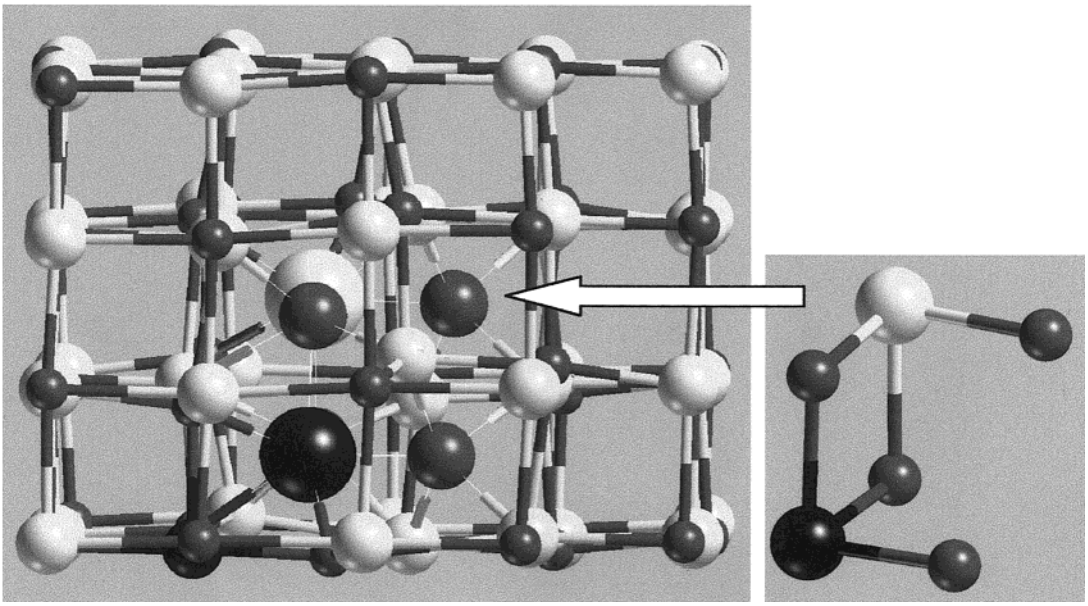

Figure 12. Ball and stick representation of a segment of the supported BaO lattice, which comprises a complex defect cluster. The cluster comprises four interstitial oxygens, an interstitial barium and strontium, an oxygen vacancy and a strontium ion occupying a barium lattice site: [Sr_{Ba}°, $Ba_i^{\bullet\bullet}$,$Sr_i^{\bullet\bullet}$, $4O_i''$, $V_O^{\bullet\bullet}$]. The interstitial ions are enlarged to enhance clarity. Barium is white, strontium is black, and oxygen is gray.

maintain coherence between the MgO and underlying $SrTiO_3$-(001). Stress reduction is facilitated, in part, by the rumpling of the MgO ions and is most pronounced at the interfacial plane diminishing further from the interface where the MgO adopts a cubic structure. O−Mg−O angles are ca. 140−160° in the [010] and [100] directions for the interfacial MgO plane with no rumpling observed on the MgO surface plane.

The MgO thin film therefore comprises cubic regions (rumpled interfacial structure) associated locally with a ca. +7% misfit and neighboring pseudohexagonal regions (corrugated interfacial structure) associated with a −0.5 to −4% misfit. Clearly, the strain within these regions remains high. However, upon closer inspection of the structure, a "spill over" of MgO is observed from rocksalt regions (positive misfit) into pseudohexagonal regions (negative misfit) reducing further the strain (locally) within the MgO lattice.

The average Mg−O bond distances within the thin film is calculated (RDF) to be 2.01 Å, which suggests the MgO accommodates more strain compared with the analogous MgO/$SrTiO_3$(SrO terminated) system. Such strain within the system cannot be sustained and therefore as the thickness of the thin film increases, so dislocations would evolve. Chern and Cheng also observed a corrugation of the MgO overlayer[21] and found that "the corrugation has some kind of transition state before the film reaches a truly relaxed form".

High quality MgO thin films have been fabricated on $SrTiO_3$ using molecular beam epitaxy.[21,23,24] In particular the authors find that the Mg and O ions locate on top of the substrate O and Ti ions respectively in accord with our findings. Moreover, Moller et al. conclude that initially the deposition may be considered as a selective magnesium oxide deposition onto the TiO_2 terminated planes of the $SrTiO_3$(100) surface.[24] In this present study, our calculations suggest that the TiO_2 terminated MgO/$SrTiO_3$ is energetically more stable compared with the analogous SrO terminated system (Table 1).

A theoretical study by Recio et al.[25] suggests that for small $(Mg_3O_3)_n$ clusters, hexagonal ("tubes") rather than cubic symmetry is energetically favorable for small values of *n*. As *n* increases, the energy difference is reduced until the cubic structure becomes energetically favorable. We suggest that at greater thin film thicknesses the pseudohexagonal structure of the MgO cannot be sustained and the thin film will revert to a rocksalt type structure presumably with the evolution of dislocations to help accommodate the lattice misfit. In addition, Rabier and Puls explored, using atomistic simulation techniques, diffusion in MgO[26] along MgO "pipe" structures similar to the ("pseudohexagonal") structures observed here.

We now consider the BaO/$SrTiO_3$(001) system, which is associated with a +34% lattice misfit.

BaO/$SrTiO_3$(001): SrO Terminated. The interfacial structure for the BaO/$SrTiO_3$(001) (SrO terminated) system is depicted in Figure 11. In this figure, part of the BaO has been "cut away" to show more clearly the 45° rotation of the BaO with respect to the underlying $SrTiO_3$. The supported BaO thin film accommodates the rocksalt type structure and exposes the (001) plane at both the interface and the surface of the thin film. The number of layers within the BaO thin film is ca. 7−8 with the surface comprising many steps, edges, and small BaO clusters.

Epitaxy. In contrast to the MgO/$SrTiO_3$(001) system, the Ba and O species lie directly above the corresponding O and Sr counterions of the $SrTiO_3$ support demonstrating such registry over the entire interfacial region. Essentially the BaO may be regarded as having rotated by 45° relative to the underlying $SrTiO_3$ surface (see for example Figure 6). In addition, no dislocations are present within the BaO thin film structure.

Chern and Cheng, who investigated experimentally the SrO/$SrTiO_3$(001) system, found the SrO rotated by 45° compared with the analogous MgO/$SrTiO_3$(001) system.[21] Since the lattice parameter for the SrO is higher compared to MgO (5.2 and 4.2, respectively) the associated lattice misfit for the SrO to accommodate the same configuration as for MgO on $SrTiO_3$ would be +28% compared with +14% for the rotated configuration. For the BaO/$SrTiO_3$ system the lattice misfit associated with this 45° rotation ($a_o(BaO) = \sqrt{2}a_o(SrTiO_3)$) is lower still at −0.3% ($a_{o(BaO)} = 5.5$ Å). It is likely therefore that the real BaO/$SrTiO_3$ system would, as we have predicted, exhibit such a rotation and we await experimental confirmation. Moreover, such a low misfit suggests that the strain within the thin film is low and thus the critical thickness is likely to be high. It is not

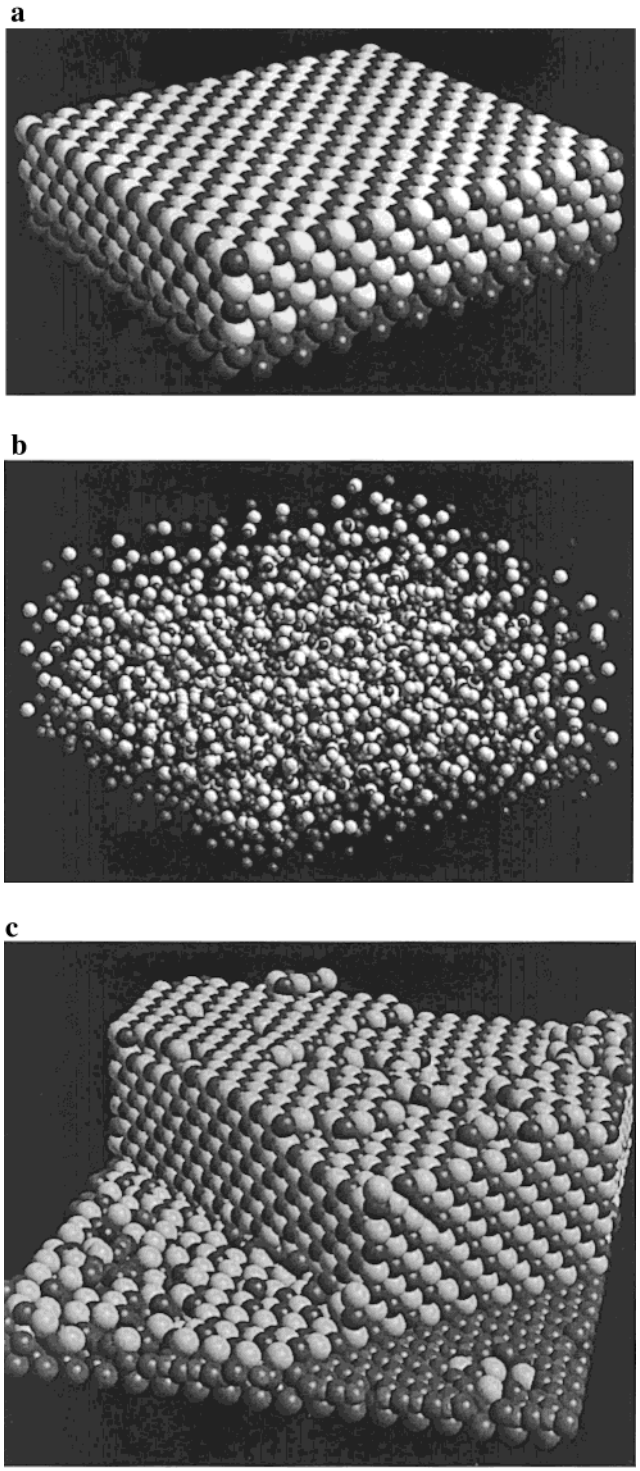

Figure 13. Sphere representations of the $BaO/SrTiO_3(001)$ (TiO_2 terminated) system. Only a small part of the full simulation cell is depicted for reasons of clarity: (a) initial structure; (b) amorphous structure after 150 cycles of dynamical simulation, and (c) final structure where part of the overlying BaO thin film has been cut away to demonstrate more clearly, the 45° rotation of the BaO lattice with respect to the underlying $SrTiO_3$. Barium is represented by the white spheres, oxygen the dark spheres. The sizes of the ions for part b has been reduced in comparison to parts a and c to illustrate more clearly the amorphous structure.

surprising therefore that misfit-induced dislocations do not feature within the BaO thin film.

Defect Structure. Structural inspection of the $BaO/SrTiO_3$ reveals defects within the BaO thin film. These include isolated Ba and O vacancies (a Ba vacancy is shown in Figure 11), associated vacancies including Ba,O pairs, triplets (Ba,O,Ba) and larger vacancy clusters including Ba_6O_5. The latter can perhaps be described as a void or cavity within the BaO thin film similar to those identified by Dong et al.[18] In addition, intermixing of Ba and Sr occurs across the interface with the Ba ions occupying Sr positions within the $SrTiO_3$ support. The Sr ions displaced occupy Ba lattice positions within the BaO thin film in addition to interstitial positions. Close inspection of the thin film structure reveals several Ba and O ions occupy interstitial positions within the BaO lattice associated with vacancies. One particularly complex defect cluster is depicted in Figure 12 and can be classified, using Kroger−Vink notation as $[Sr_{Ba}^{o}, Ba_i^{\bullet\bullet}, Sr_i^{\bullet\bullet}, 4O_i'', V_O^{\bullet\bullet}]$.

$BaO/SrTiO_3(001)$: TiO_2 Terminated. To illustrate the amorphization and recrystallization methodology, the starting structure for the $BaO/SrTiO_3(001)$ system is depicted in Figure 13a where the BaO thin film is constrained to accommodate a 34% reduction in lattice parameter such that the BaO lies coherent with the underlying $SrTiO_3(001)$ support. Imposing dynamical simulation upon the system results in the amorphization of the BaO thin film, which is depicted in Figure 13b. The figure shows a snapshot of the evolving structure taken after 150 cycles of dynamical simulation. Prolonged dynamical simulation followed by "energy minimization" (dynamical simulation performed at 0 K), results in the recrystallization of the BaO thin film. This system was chosen to illustrate the amorphization and recrystallization since the amorphized structure of the $BaO/SrTiO_3$ is more striking owing to the greater thickness of the BaO thin film and the final structure (TiO_2 terminated system) comprises dislocations.

The final interfacial structure for the $BaO/SrTiO_3(001)$ (TiO_2 terminated) is presented in Figure 13c. The supported BaO thin film accommodates the rocksalt type structure and exposes the (001) plane at both the interface and the surface of the thin film. The number of layers within the BaO thin film is ca. 7−8 with the surface comprising many steps, edges, and small BaO clusters. Again, part of the BaO has been "cut away" to show more clearly the 45° rotation of the BaO with respect to the underlying $SrTiO_3$. To the left of Figure 13c the interfacial BaO layer is depicted to show the considerable perturbation, rumpling, and highly defective nature of the plane compared with planes further from the interface, which are more coherent. Figure 14 depicts the TiO_2 and BaO interfacial planes showing more clearly the defective structure. In contrast, the $BaO/SrTiO_3$-(001) (SrO-terminated) system, considered above, shows almost no perturbation of the interfacial TiO_2 and BaO planes.

Epitaxy. For BaO supported on the TiO_2 terminated $SrTiO_3$ surface, the oxygen sublattice (BaO) lies directly above the Ti sublattice with Ba ions lying above the midpoint of the TiO_2 network (directly above the oxygen sublattice of the underlying SrO plane of the $SrTiO_3$) as depicted in Figure 14.

Dislocations. In contrast to the $BaO/SrTiO_3$ (SrO terminated) system, this system exhibits a high concentration of dislocations. For illustration, one particular dislocation is depicted in Figure 15. To maintain clarity of the dislocation core structure, part of the surrounding BaO lattice has been removed.

Conclusion

The $MgO/SrTiO_3(001)$ and $BaO/SrTiO_3(001)$ systems demonstrate markedly different structural characteristics. One of the main reasons for this is the difference in lattice misfits associated with each system. In particular, for the $MgO/SrTiO_3(001)$ system (misfit = 7.4%), the MgO is oriented at 0° with respect to the

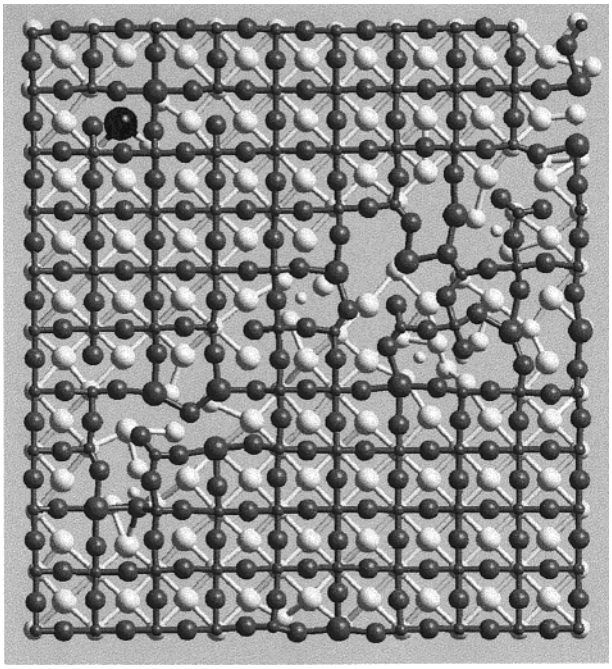

Figure 14. Ball and stick representation of the interfacial TiO_2 and BaO planes within the $BaO/SrTiO_3(001)$ (TiO_2 terminated) system. For reasons of clarity, only a small part of the full simulation cell is depicted. Barium ions are represented by the large white spheres, oxygen (BaO) the smaller white spheres, oxygen (TiO_2) the large dark spheres and titanium, the small dark spheres. Notice the strontium ion (black, top left), which has substituted for a barium ion.

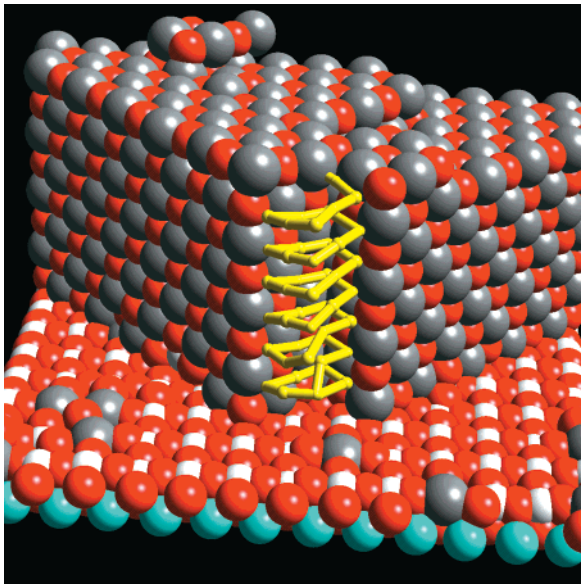

Figure 15. Sphere representation of the $BaO/SrTiO_3(001)$ (TiO_2 terminated) system depicting a dislocation (stick model, colored yellow), which has evolved within the BaO thin film. To maintain clarity of the dislocation, part of the surrounding BaO lattice has been removed. Barium is colored gray, oxygen is red, titanium is white. and strontium is blue.

underlying $SrTiO_3$ in contrast to the BaO, which undergoes a 45° rotation about an axis normal to the $SrTiO_3(001)$ surface. The latter enables the associated lattice misfit to be reduced from +34% to −0.3%.

In addition, the particular plane exposed at the surface by the $SrTiO_3$ (either SrO or TiO_2) is critical to the structural characteristics of the supported thin film. For the $MgO/SrTiO_3$-(001) (SrO terminated) system, the lattice misfit is accommodated by the presents of dislocations, while the analogous $MgO/SrTiO_3(001)$ (TiO_2 terminated) system undergoes a remarkable structural transformation, in which regions of MgO accommodate a "pseudohexagonal" type structure. The associated lattice misfit within these pseudohexagonal regions is effectively reduced from +7% to ca. −0.5 to −4%. An analogy can perhaps be drawn between the MgO and a concertina.

For the $BaO/SrTiO_3$ system the surface exposed by the $SrTiO_3$ exacts a somewhat less dramatic structural influence on the supported oxide. For the $BaO/SrTiO_3(001)$ (TiO_2 terminated) system, the BaO comprises a network of dislocations in contrast to the SrO terminated system, where no dislocations are present. In addition, while the interfacial planes within the TiO_2 terminated system suffer considerable structural perturbation, the analogous SrO terminated system demonstrates almost perfect coherence of the interfacial planes.

The study also demonstrates the applicability of our methodology (simulated amorphization and recrystallization) as applied to more complex systems than previously considered. And while our findings are supported by experiment, detailed comparisons are not possible owing to the difficulty in elucidating the precise atomistic structure of such systems experimentally. Conversely, since the simulations are capable of providing such explicit atomistic detail they offer a powerful complementary technique to experiment.

References and Notes

(1) Sutton, A. P.; Balluffi, R. W. *Interfaces in Crystalline materials*; Monographs on the Physics and Chemistry of Materials 51; Oxford University Press, Inc.: New York, 1985.
(2) Baker, J.; Lindgard, P. A. *Phys. Rev. B.* **1999**, *60*, 16941.
(3) Sayle, D. C.; Maicaneanu, S. A.; Slater, B.; Catlow, C. R. A. *J. Mater. Chem.* **1999**, *9*, 2779.
(4) Kawasaki, M.; Takahashi, K.; Maeda, T.; Tsuchiya, R.; Shinohara, M.; Ishiyama, O.; Yonezawa, T.; Yoshimoto, M.; Koinuma, H. *Science* **1994**, *266*, 1540.
(5) Sayle, D. C.; Watson, G. W. *Surf. Sci.* **2001**, *473*, 97.
(6) *Philos. Mag. B* **1996**, *73*. Special edition ("Interatomic Potentials").
(7) Ewald, P. P. *Ann. Phys.* **1921**, *64*, 253.
(8) Lewis, G. V.; Catlow, C. R. A. *J. Phys. C: Solid State Phys.* **1985**, *18*, 1149.
(9) Sayle, D. C.; Sayle, T. X. T.; Parker, S. C.; Catlow, C. R. A.; Harding J. H. *Phys. Rev. B* **1994**, *50*, 14498.
(10) Watson, G. W.; Kelsey, E. T.; Parker, S. C. *Philos. Mag. A* **1999**, *79*, 527.
(11) Harris, D. J.; Watson, G. W.; Parker, S. C. *Philos. Mag. A* **1996**, *74*, 407.
(12) Sayle, D. C.; Watson, G. W. *J. Mater. Chem.* **2000**, *10*, 2241.
(13) Kenway, P. R.; Oliver, P. M.; Parker, S. C.; Sayle, D. C.; Sayle, T. X. T.; Titiloye, J. O. *Mol. Simul.* **1992**, *9*, 83.
(14) DL_POLY is a package of molecular simulation routines written by W. Smith and T. R. Forester. Copyright: The Council for the Central Laboratory of the Research Councils, Daresbury Laboratory, Daresbury, Warrington, UK, 1996.
(15) Grzybowski, A.; Gwozdz, E.; Brodka, A. *Phys. Rev. B* **2000**, *61*, 6706.
(16) Schnitker, J.; Srolovitz, D. J. *Model. Simul. Mater. Sci. Eng.* **1998**, *6*, 153.
(17) Jain, S. C.; Harker, A. H.; Cowley, R. A. *Philos. Mag. A* **1997**, *75*, 1461.
(18) Dong, L.; Schnitker, J.; Smith, R. W.; Srolovitz, D. J. *J. Appl. Phys.* **1998**, *83*, 217.
(19) Levay, A.; Mobus, G.; Vitek, V.; Ruhle, M.; Tichy, G. *Acta Mater.* **1999**, *47*, 4143.
(20) Sayle, D. C.; Catlow, C. R. A.; Harding, J. H.; Healy, M. J. F.; Maicaneanu, S. A.; Parker, S. C.; Slater, B.; Watson, G. W. *J. Mater. Chem.* **2000**, *10*, 1315.
(21) Chern, G.; Cheng, C. J. *Vac. Sci. Technol. A* **1999**, *17*, 1097.
(22) Sutton, A. P.; Balluffi, R. W. *Acta Metal.* **1987**, *35*, 2177.
(23) Stampe, P. A.; Kennedy, R. J. *J. Cryst. Growth* **1998**, *191*, 478.
(24) Moller, P. J.; Komolov, S. A.; Lazneva, E. F. *Surf. Sci.* **1999**, *425*, 15.
(25) Recio, J. M.; Pandey, R.; Ayuela, A.; Kunz, A. B. *J. Chem. Phys.* **1993**, *98*, 4783.
(26) Rabier, J.; Puls, M. P. *Philos. Mag. A* **1985**, *52*, 461.